Electrochimica Acta 55 (2010) 7975–7981

Contents lists available at ScienceDirect

Electrochimica Acta

journal homepage: www.elsevier.com/locate/electacta

The oxygen reduction reaction mechanism on Pt(1 1 1) from density functional theory calculations

Vladimir Tripković[a], Egill Skúlason[a], Samira Siahrostami[a,b], Jens K. Nørskov[a], Jan Rossmeisl[a,*]

[a] Center for Atomic-scale Materials Design (CAMD), Department of Physics, Technical University of Denmark, Kgs. Lyngby 2800, Denmark
[b] Department of Chemistry, College of Sciences, Shiraz University, Shiraz 71454, Iran

ARTICLE INFO

Article history:
Received 7 December 2009
Received in revised form 15 February 2010
Accepted 18 February 2010
Available online 25 February 2010

Keywords:
Oxygen reduction reaction
Pt
DFT
Reaction mechanism

ABSTRACT

We study the oxygen reduction reaction (ORR) mechanism on a Pt(1 1 1) surface using density functional theory calculations. We find that at low overpotentials the surface is covered with a half dissociated water layer. We estimate the barrier for proton transfer to this surface and the barrier for proton transport parallel to the surface within the half dissociated water network. We find both barriers to be small. The only potentially dependent step is the proton transfer from water to the half dissociated water layer. We find that ORR proceeds via four direct e^- reductions without significant peroxide formation. We show that the oxygen–oxygen bond breaking is dependent on the local surface environment. The minimum energy pathway is constructed and we confirm that OH removal from the surface determines the overpotential.

1. Introduction

The largest challenge in the proton-exchange membrane fuel cell (PEMFC) catalysis is to reduce the amount of Pt needed at the cathode. The cathode contains 80–90% of the total amount of Pt used in PEMFC. Sluggish kinetics at the cathode accounts for the major part of voltage drop in PEMFCs. This limits state-of-the-art systems to operate at voltages of only ~0.7 V, far from the equilibrium potential of ~1.2 V [1]. To make fuel cell production economically viable, one has to increase the mass activity of Pt by at least factor of four [1].

Deducing a reaction mechanism from the measured kinetics is a tremendously difficult problem [2,3]. In that perspective DFT studies have provided huge molecular level understanding of surface phenomena that are taking place during the ORR. The DFT simulations enabled us to relate the binding energies of all the intermediates in the ORR to the binding energy of oxygen [4] and use that knowledge to construct an activity volcano [5] depending just on that single descriptor. The activity volcano is limited by two rate determining steps; OH removal and OOH formation on the surface [3,6]. Therefore ideally it would be desirable to have weaker OH and stronger OOH binding to the surface. Since one cannot change independently binding energies of OH and OOH, material with the tradeoff of these two limiting regimes will be the best catalyst for this reaction. Pt with an intermediate O binding energy is found to be close to the top of the volcano explaining why it stands out as the best single element catalyst. Higher activities can be reached by slightly tuning the oxygen binding energy by alloying Pt with some other metal [7,8]. However, these previous theoretical studies relied on the binding energies of the most stable intermediates, and it was implicitly assumed that any additional reaction barriers are rather small or essentially potential and metal independent.

The barriers for O_2, OOH and HOOH bond breaking on the pure Pt(1 1 1) surface have been calculated by Nilekar and Mavrikakis in the absence of water and an applied bias [9]. The first charge transfer reaction of the ORR has also been modeled previously by Janik et al. in a water environment at a constant surface charge [10]. This study showed that the barrier for this reaction is very small. The reaction was modeled having water at the surface; however, at the potentials where the ORR takes place, the electrode surface will start to oxidize. Therefore the OH coverage will be substantial and this could significantly affect the results [11].

In the present we study the ORR mechanism at relevant potential, at a realistic surface coverage of OH and in the presence of water. First we calculate the binding energy of hydroxyl as a function of the OH coverage; from this we determine the coverage of OH at potentials of interest to be 1/3 ML. Subsequently we model all ORR intermediates in this H_2O/OH hydrogen bonded network.

2. Method

All the electronic structure calculations have been carried out using density functional theory, using the RPBE functional for

* Corresponding author.
E-mail address: jross@fysik.dtu.dk (J. Rossmeisl).

0013-4686/$ – see front matter © 2010 Elsevier Ltd. All rights reserved.
doi:10.1016/j.electacta.2010.02.056

exchange and correlation [12]. The optimized RPBE lattice constant of Pt of 4.02 Å was used. The Pt(1 1 1) electrode was represented by periodically repeated 3 layer slabs separated by 12 Å of vacuum. Test with a 5-layer slab gave similar binding energies (within ~0.07 eV per water layer). Various unit cell sizes (3×4), (6×3), (6×4), and (6×6) sampled with $(3\times2\times1)$, $(2\times4\times1)$, $(2\times3\times1)$, and $(2\times2\times1)$ Monkhorst–Pack k-point sampling grid [13] were used throughout this work. Symmetry has been used to further reduce number of k-points. The dipole correction was used in all cases to decouple the electrostatic interaction between the periodically repeated slabs. The Kohn–Sham equations were solved using a plane wave basis with a plane wave and density cutoff of 26 Ry. Ionic cores are described with Vanderbilt ultrasoft pseudopotentials [14]. A Fermi smearing of 0.1 eV was used and energies were extrapolated to an electronic temperature of 0 K. The two bottom layers of the slab were fixed in their bulk positions, while the top layer together with adsorbates was allowed to relax until the sum of the absolute forces was less than 0.05 eV $Å^{-1}$. Transition states were located using nudged elastic band method [15,16]. In addition to the standard RPBE calculations, we investigated the effect of including van der Waals interaction by performing calculations of the water layer using the vdW-DF functional [17,18]. All calculations were performed using Dacapo [19], GPAW [20] and ASE simulation package [21].

3. Results and discussions

The outline of this section is as follows. First we investigate the half dissociated water layer. We calculate the differential adsorption energy of OH on Pt(1 1 1) surface shown in Fig. 1. We discuss and estimate the barriers for proton transfer from the electrolyte to the OH on the surface and surface proton diffusion, in Figs. 2 and 3, respectively. We illustrate a possible reaction mechanism in Fig. 4

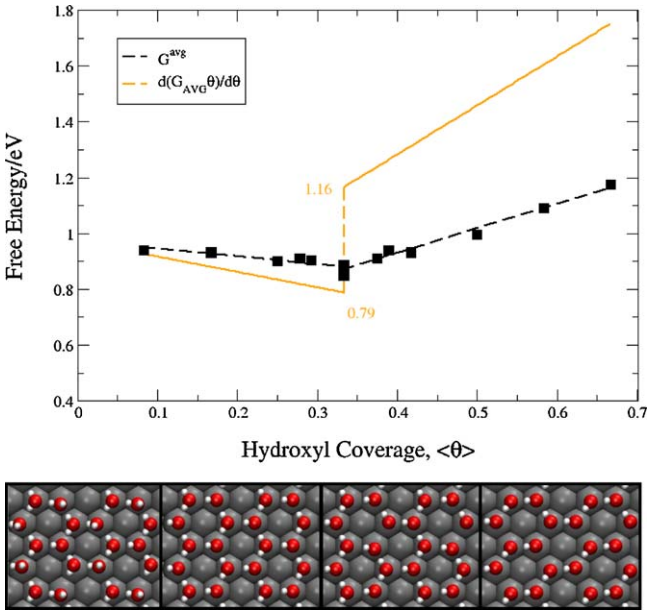

Fig. 1. (a) Average free adsorption energy of hydroxyl species on Pt(1 1 1). Discrete values (black squares) are linearly fitted (black dashed line) from low and high coverage end to 1/3 of hydroxyl coverage. Fits are used to get the differential adsorption energy of OH on the surface (yellow line). Dashed yellow line represents the discontinuity in the differential free energy at 1/3 ML hydroxyl coverage. Differential free energies of hydroxyl at different ends of discontinuity, 0.79 and 1.16 eV are also indicated. (b) Top view of four representative OH coverage structures, at very low hydroxyl coverage (0.08 ML), at different ends of discontinuity (0.33 and 0.42 ML) and at very high hydroxyl coverage (0.66 ML), in the order from left to right, respectively.

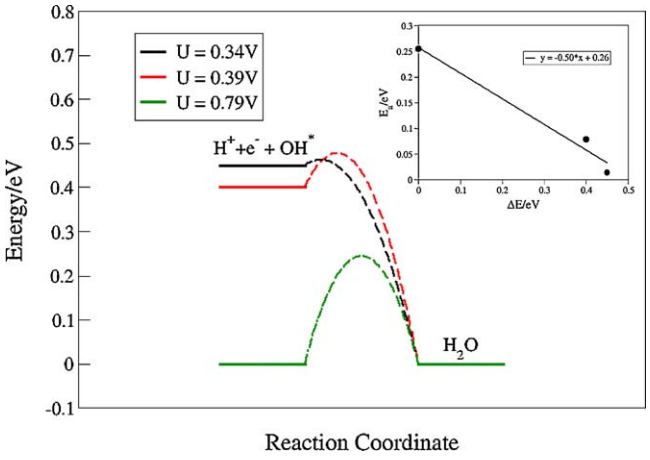

Fig. 2. Potential energy profiles for reducing one OH in the half dissociated water network by proton in the second water layer at three different initial potentials. The potential does not change much during the proton transfer reaction. Inset shows Brønsted–Evans–Polanyi (BEP) relationship for the charge transfer to the surface OH. Transfer coefficient (BEP slope) and the reaction barrier at the equilibrium are 0.5 and 0.26 eV, respectively.

and finally in Figs. 5 and 6 we construct the free energy diagram (FED) of the minimum reaction path taking proton transfer and surface diffusion into account.

3.1. OH coverage

It has been found both experimentally [22,23] and theoretically [22,24,25] that the most stable water structure forms a honeycomb $(\sqrt{3}\times\sqrt{3})$R30 pattern with 2/3 ML water coverage. This water bilayer structure consists of two differently coordinated water molecules; where one is parallel to the surface and the other water molecule has an O–H bond pointing towards/away from the surface. These two structures have the same stability within a few meV [22,26–29]. Water can easily react with oxygen on the surface to form OH maintaining the honeycomb structure [28]. A water phase where every second water molecule has dissociated to OH has been named the half dissociated water structure. This particular water phase was found to be the most stable one up to 160 K under UHV conditions [30]. This stability stems from very strong OH–H_2O hydrogen bond [31,32]. The number of these bonds is maximized in this structure because every OH is bonded to three adjacent water molecules.

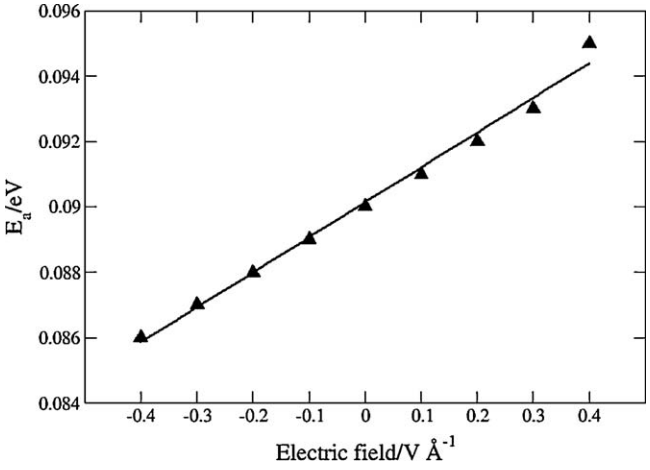

Fig. 3. The transition state energy for proton diffusion within the half dissociated water layer as a function of the applied field. Dipole moment perpendicular to the surface is very small, 0.011 eÅ, indicating that this step is potential independent.

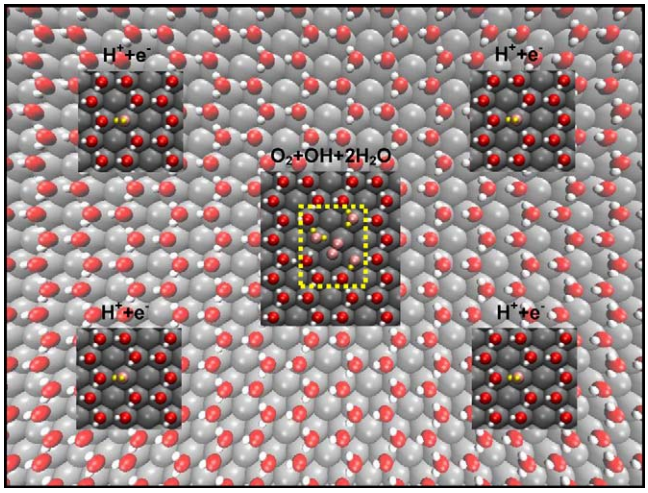

Fig. 4. Schematic illustration of the reaction mechanism. Surface is covered with half dissociated water network (transparent background). Four additional hydrogen atoms indicated (left and right panels). These atoms can easily diffuse to the reaction center (middle panel) where they reduce ORR intermediates. The dashed yellow box in the middle panel represents the simulated unit cell. All the structures are shown embodied in the half dissociated water network.

Under electrochemical conditions, cyclic voltammograms for Pt(1 1 1) show an oxidation peak around 0.8 V vs. reversible hydrogen electrode (RHE) (from simulation point of view there is no difference between the reversible and the standard hydrogen electrode [33]). This peak is believed to be related to the splitting of water into adsorbed OH^* and $H^+ + e^-$ [34,3]. It is difficult to get the exact surface structure via *in situ* experiments. However, infrared spectroscopy suggests that the water on Pt(1 1 1) is in an ice-like structure [35]. From DFT simulations of the oxidation peak in cyclic voltammograms, charge seems to be well reproduced by assuming an isotherm with the half dissociated water layer [2,29].

In the next section we will be looking at the three different free energies schemes for OH adsorption; average, integral and differential free energy scheme. The average free energy of OH is defined as the average adsorption energy per number of OHs, n, in the simulated cell. This energy shows the strength of the interaction between the adsorbed OH species. On the other hand, integral free energy is the total OH adsorption energy normalized with the respect to the size of the simulated cell or equivalently number of the surface atoms, N, in the simulation. It is obtained by multiplying the average free energy with the OH coverage. Besides this energy equals the energy stored in a capacitor set up between surface adsorbed water layer and the slab. Differential free adsorption energy is obtained by differentiating the free integral energy with respect to the OH coverage. Differential adsorption energy shows the most stable surface structure at corresponding potential. The relationship between the three different energy schemes is given in Eq. (1).

$$\frac{dG}{N\,d\theta} = \frac{d(G^{avg}\theta)}{d\theta} = \frac{d(G^{int})}{d\theta}, \quad \theta = \frac{n}{N} \tag{1}$$

The average free energy of OH species as a function of coverage is presented in Fig. 1 (black squares). We start by stepwise removing H atoms from the water bilayer. When 1/3 ML of OH coverage is reached, further increase of the OH concentration can only be achieved by taking one of the hydrogen atoms from the water molecules in plane with the surface. This equals to removing one of the hydrogen bonds. 2/3 of OH coverage is reached when one hydrogen atom has been abstracted from all water molecules. We note here that this high OH coverage is unrealistic under electrochemical conditions and that oxide layer will instead build up on the surface at higher potentials [11,36].

Free average energy adsorption profile (dashed black line) is obtained by linearly fitting discrete points from both, low and high coverage end to the coverage of 1/3 ML of hydroxyl. It can be seen from Fig. 1 that OH–OH interaction has a kink in the middle, meaning that the interaction is attractive below 1/3 ML and repulsive above 1/3 ML.

There are two ways in which we can calculate the adsorption energy of OH. We will illustrate this on the example of the integral energy. The first way is to compare the adsorption energies of OH on the surface to the liquid water and hydrogen molecules in the gas phase, whereas water in the bilayer is used as a reference for water molecules. Zero point energy and entropy correction are added to get the free adsorption energy at 300 K ($G = E + ZPE - TS$).

$$E_{OH}^{int} = E\left(\theta OH + \left(\frac{2}{3} - \theta\right) H_2O\right) - E_{slab} - \frac{2}{3}E(H_2O) + \frac{1}{2}\theta E(H_2) - \left(\frac{2}{3} - \theta\right)(E(H_2O*) - E_{slab} - E(H_2O)) \tag{2}$$

Here $E(H_2O^*)$ is the average energy of a water molecule in the water bilayer on the surface.

Another more direct way of calculating the adsorption energy is:

$$E_{OH}^{int} = E\left(\theta OH + \left(\frac{2}{3} - \theta\right) H_2O\right) - E_{slab} + \frac{1}{2}\theta E(H_2) - \frac{2}{3}E(H_2O*) \tag{3}$$

Table 1
Dissociation barriers and bond lengths for the most stable oxygen species on Pt(1 1 1) slab coordinated to different number of water molecules. Bond length for O_2 in vacuum from RPBE-DFT calculation is also included for comparison.

	E^{diss}/eV	Bond length/nm
O_2 (g)		0.124
O_2 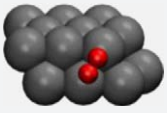	0.73	0.135
$O_2 + H_2O$ 	0.67	0.140
$O_2 + 2H_2O$ 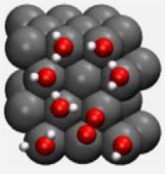	0.48	0.142
OOH[a] $+ 2H_2O$ 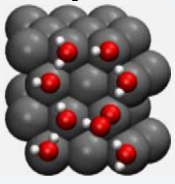	0.37	0.144

[a] In this case OOH is the most stable oxygen species on the surface.

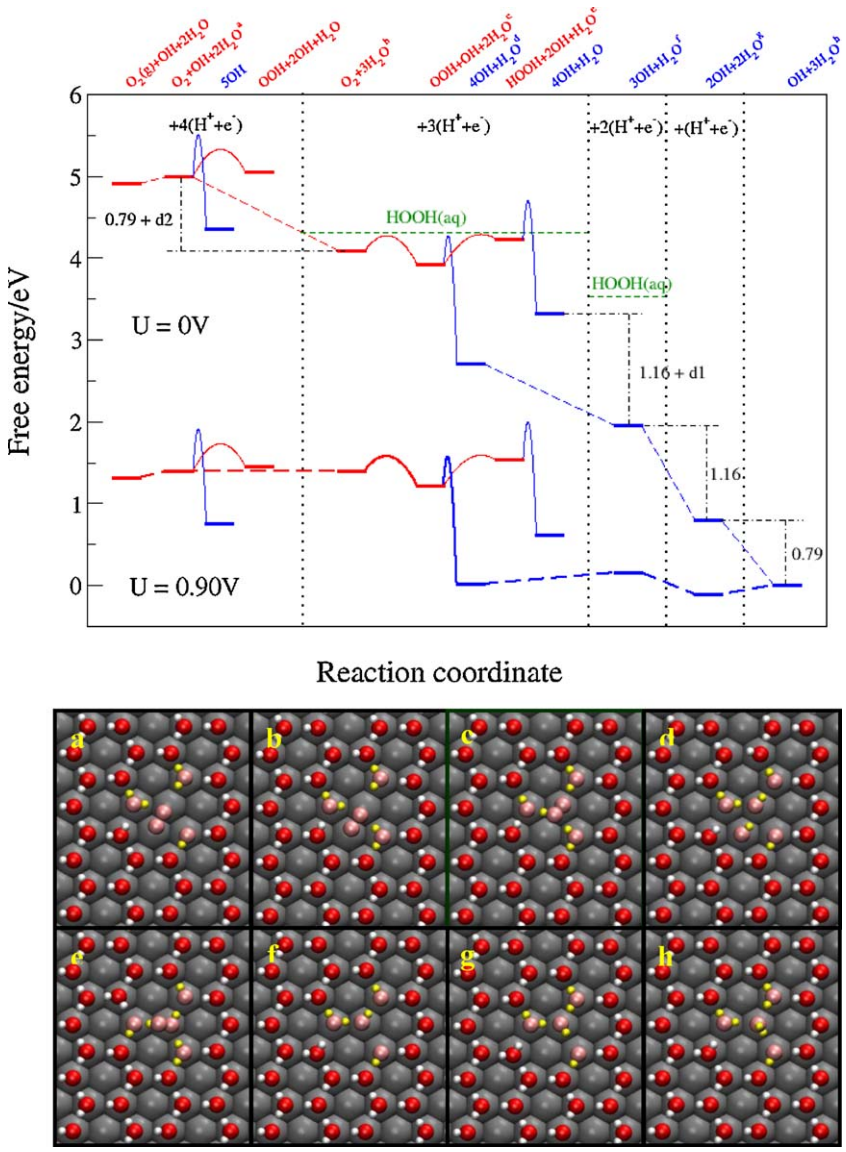

Fig. 5. (a) Free energy diagram for O_2 reduction at two different potentials, 0 (upper) and 0.9 V (lower), respectively. Red color indicates the associated species and the barriers between them. Blue color indicates dissociated species and the barriers for dissociation. Local structures are indicated above the figure panel following the same color code as the species they designate. Labels a–h correspond to the structures in b. Only the species in the reactive center are designated. Other species are left out for the sake of transparency. The thin solid and dashed lines represent the chemical and electrochemical reaction steps. At 0 V peroxide level in aqueous solution after first and second proton transfer is also indicated (green dashed line). Different electrochemical steps are fixed to the values (0.79 eV, 1.16 eV) from Fig. 1 in the way explained in the text. d1 (0.21 eV) and d2 (0.12 eV) represents the effect of (de)stabilization or equivalently energy difference between the structure in the reaction path and the most stable structure with same number of species (one in Fig. 1). Minimum energy path is highlighted at 0.9 V. (b) The most important intermediate structures on the ORR potential energy landscape embodied in the half dissociated water layer network, labeled from a–h. Pt(1 1 1) slab, oxygen and hydrogen atoms are colored in dark gray, red and white, respectively. Oxygen and hydrogen atoms designated in the FED are colored in pink and yellow, respectively.

This corresponds to using the water in the bilayer as a reference for OH instead of the liquid water and H_2 in the gas phase. If the water bilayer was in equilibrium with liquid water, Eqs. (2) and (3) would give the same result. The challenge is that in the standard GGA simulations the stability of water in the bilayer is underestimated mainly due to lack of van der Waals forces. This means that the potential for water oxidation will also be underestimated. We find that including the van der Waals interactions within the water layer and between the water layer and the surface, stabilize each water molecule with ~0.15 eV compared to the standard RPBE-GGA calculations. This brings the oxidation potential calculated with Eq. (3) close to the potential calculated with Eq. (2). In the following we therefore use first of the two methods for calculating adsorption energies.

Differentiating the integral free energy (see Eq. (1)) we get the differential free energy of the hydroxyl species on the surface (yellow line). The kink in the average free adsorption energy becomes a discontinuity (yellow dashed line) in the differential free adsorption energy.

The differential free energy of OH at different ends of the discontinuity at 1/3 coverage is 0.79 and 1.16 eV, respectively. We conclude from these values that adding/removing $H^+ + e^-$ to/from the half dissociated water differs by 0.37 eV. This is in agreement with previous DFT studies on the OH–H_2O structure [31,32].

We apply the computational standard hydrogen electrode (SHE) [5] to convert the differential free energy scale into an electric potential scale in a similar way as it was done previously for hydrogen adsorption [37].

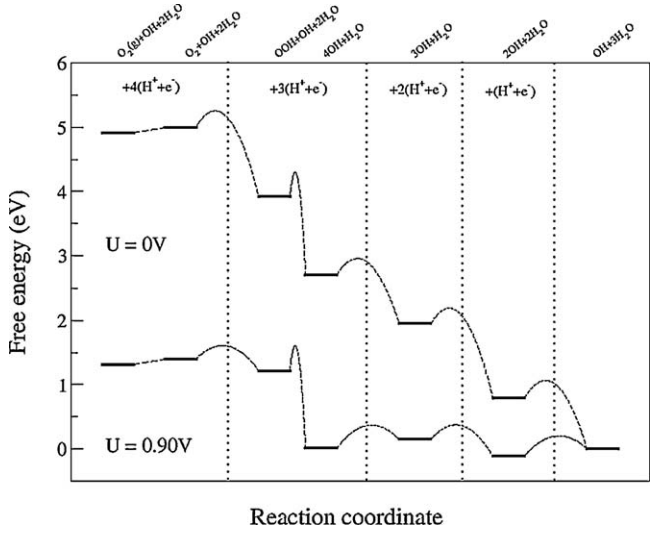

Fig. 6. Simplified free energy diagram for O_2 reduction at 0 V (upper) and 0.9 V (lower) potential. The most stable states in each electrochemical step together with the minimum reaction barrier for splitting the O–O bond are indicated. Electrochemical reduction steps are separated by dashed vertical lines. Barriers for proton transfer to the reaction center in the electrochemical steps (0.26 eV) are indicated with dashed black lines.

In that way, Fig. 1 can be interpreted as the potential needed to oxidize the OH–H_2O layer at a given coverage. We will use the differential free energy of hydroxyl at both ends of the discontinuity in Fig. 1 to fix the free energy levels of the different electrochemical steps in the FEDs in Figs. 5 and 6.

3.2. Charge transfer and surface diffusion

Before discussing the ORR mechanism in detail, a few issues regarding proton transfer and surface diffusion will be addressed. The half dissociated water network on the surface can also be viewed as the inner Helmholtz plane in the classical description of the double layer. In this picture the diffuse part or the outer Helmholtz plane of the double layer is set up between a charged water layer and the half dissociated water layer on the surface. Most of the potential drop will take place in the inner Helmholtz plane, because experimental isotherm obtained from integrated CV measurements for Pt(1 1 1) agrees well with the simple binding model of OH on the surface [29]. Therefore surface charge will not be significantly affected by proton concentration in the charged second water layer, opposite to what was found in the hydrogen evolution/oxidation region [38]. In order to mimic proton transfer at high potentials relevant for ORR one has to use very large simulation cells.

We simulate the reduction of the half dissociated water layer in the following approximate way. The largest unit cells we are able to model correspond to 0.79 V (equilibrium potential). In Fig. 2 we present results at three different potentials. For the point at the equilibrium (green line) we find a barrier of 0.26 eV for proton transfer. We note that a previous DFT study also found a low additional barrier for proton transfer to adsorbed oxygen molecule on Pt(1 1 1) surface [10]. Transfer coefficient for this charge transfer reaction is found to be 0.5, and since this is the only step that is potential dependent in the ORR, this will be the overall charge transfer coefficient. This result agrees perfectly with the experimental value of 0.5 [41].

Proton diffusion parallel to the surface occurs readily through interchange of hydrogen bonds within the water network. We get a 0.09 eV barrier for proton diffusion in the dissociated water network. Very low diffusion barriers have also been reported elsewhere [39]. In Fig. 3 we show the influence of an electric field on the transition state energy for the proton diffusion. We found very small changes of 0.01 eV in the activation energy in the large electric field range between −0.4 and +0.4 V $Å^{-1}$. Therefore we consider proton diffusion as a field and potential-independent step.

We will take the larger of the two barriers (0.26 eV) for the barrier needed to transport proton from the bulk water to the specific site on the surface where ORR takes place. This barrier will be used in the last part of this section to construct simplified FED in Fig. 6.

3.3. Reaction path model

A schematic illustration of the proposed reaction mechanism is shown in Fig. 4. Charge transfer is decoupled from the surface reaction in the following way: (1) a proton is transferred to OH somewhere on the surface where it picks up an electron; (2) the proton can then diffuse independently of the potential to the adsorbed oxygen molecule; and (3) reduce it. This process is repeated four times until the oxygen molecule has been reduced to two water molecules. The potential dependent charge transfer reaction is the same in all four steps with a rather small additional barrier (0.26 eV). We note that direct transfer of a proton to the adsorbed oxygen could also be a possible route, but this would only reduce the barrier relative to what is found in this paper. Since this barrier is already small enough, this will not affect conclusions of this study.

3.4. The free energy diagram

Fig. 5 is constructed from the adsorption energies of different ORR species and the differential free energy of OH. Since ORR is taking place just on specific sites on the surface, we assume that the global OH coverage remains constant. Therefore by locally changing OH coverage as a consequence of ORR, we can just infinitesimally move away from the global surface coverage of 1/3 ML of OH. We analyze the free energy diagram at $U = 0$ V backwards, starting from the last electrochemical step. The difference between the two states in the last electrochemical step is set to 0.79 eV, or the lower value in the discontinuity in Fig. 1. This value corresponds to a subtraction of one H^+ and e^- from H_2O at local OH coverage below 1/3 ML and forming the half dissociated water network, hence infinitesimally increasing the global OH coverage to 1/3 ML. In other words, water dissociation will become feasible at potentials greater than 0.79 V. In the same way are the second and the third electrochemical step set to 1.16 eV; the value at the other end of discontinuity, since we are now removing one $H^+ + e^-$ and hence increasing the OH coverage infinitesimally above 1/3 ML. The fourth electrochemical step is set to 0.79 eV between the two states with the adsorbed oxygen on the surface under different local OH coverage. Again this is because we remove one $H^+ + e^-$ near the adsorbed oxygen molecule where both states are below 1/3 ML of OH coverage. States that we get from our reaction mechanism can have different orientation of adsorbed species on the surface than the most stable structures with the same species. Therefore one also needs to correct for the difference between the most stable structure with certain OH coverage (ones in Fig. 1) and the ones obtained as a product of the reaction mechanism in the FED (d1 and d2 in Fig. 5).

First, we construct the FED at 0 V. We can obtain the FED at any desired potential by shifting the relative positions of all states at $U = 0$ V by the chemical potential of the electrons. We shift the states to 0.9 V potential since this is a potential relevant for ORR and within the potential window where the half dissociated water layer is stable.

The O_2 adsorption will be the first step in the FED. The O_2 level in the gas phase is fixed to a value of 4.92 eV compared to the liquid water and hydrogen in the gas phase. This value corresponds to a maximum work one can get out from the system.

There are two possible reaction paths after initial O_2 adsorption. O_2 can either react with one proton and electron from the surrounding water molecules to form OOH, or dissociate. The relative stability of the O_2 and OOH depends on the local OH coverage. After proton transfer to the OH in the vicinity of O_2, dissociation becomes more facile. This is related to water at the surface being a stronger proton donor than OH [31,32]. Dissociation barriers and bond lengths depending on the number of hydrogen bonds coordinated to the most stable oxygen species are tabulated in Table 1. For O–O bond scission compared to the most stable intermediate, we get the lowest barrier to be 0.37 eV which is considerably less than 0.73 eV we find on the bare Pt(1 1 1) surface. If we include the electric field correction for transition state for O_2 dissociation at 0.9 V from Ref. [40], barrier will shift upwards by additional 0.06 eV.

OOH species can further react with nearby water molecules to form HOOH. This reaction step is energetically unfavorable which is in agreement with rotating ring disc experiments where only traces of peroxide are present at ORR relevant potentials [41]. The hydrogen peroxide energy level in aqueous solution [42] is also indicated for comparison with the green dashed line in the second and the third panel in Fig. 5. Difference between the two peroxide levels in aqueous solution is 0.79 eV due to the way the FED was constructed.

This analysis confirms our previous established thermodynamically picture that OOH is the most stable reaction intermediate after first reduction step. As a product of O–O bond scission we can either get O or 2OH since the nearest water molecules can donate a hydrogen atom to oxygen to form 2OH. We find very similar reaction energies and activation barriers for these two mechanisms. This is a result of simple scaling relationships that exist between different oxygen species based on the number of bonds each species has to the surface [4,43]. Consequently the difference in the free energy between O and 2OH is independent on material.

The following three consecutive electrochemical steps are simple proton transfer steps. In the final structure there is one more water molecule due to an extra hydrogen atom sitting on top of one OH in the half dissociated water layer. This additional water molecule can be readily replaced by O_2 [44], thus completing the catalytic cycle.

The barrier for breaking the oxygen–oxygen bond is potential independent, which means that it will not show up in comparing activities at different potentials. This is the reason why the analysis based on the intermediates binding gives qualitatively correct polarizations curves [2]. However, the barrier might change when the catalyst is changed, this could affect the previously established volcano curves. We speculate that less reactive catalysts might be predicted too active compared to Pt without explicitly including the kinetics.

The most stable intermediate in each electrochemical step is shown in Fig. 6, a simplified version of Fig. 5. The minimum energy barrier for OOH dissociation is also indicated as well as the barriers for charge transfer between different electrochemical steps. At $U = 0.9$ V from Fig. 6 OOH formation and OH removal step have very similar barriers. We speculate that inclusion of more water (larger unit cells) could slightly stabilize OOH and OH at surface. Any stabilization would reduce the barrier for OOH dissociation and increase the barrier for H_2O formation. This is in agreement with previous theoretical results on Pt(1 1 1) [5], where the rate of OH removal determined the overall ORR activity.

4. Conclusions

In summary we have calculated the reaction path and barriers for ORR on Pt(1 1 1). We would like to highlight that this approach differs from others in that we take explicitly into account the half dissociated water layer on the surface. All ORR intermediates are modeled within this water network, where water is not just accounted for stabilization effect it exerts on surface intermediates, but also it is directly involved in the reaction mechanism. We have constructed differential adsorption energy diagram and we have determined the most stable surface structure at potentials of interest for ORR reduction. We find that there is a discontinuity in the chemical potential at 1/3 ML of OH coverage which corresponds to energy needed for removing one extra hydrogen atom from the half dissociated water layer network. From this we have constructed the FED for O_2 reduction on Pt(1 1 1) at 0.9 V. The results are in agreement with the previously established picture that on Pt(1 1 1), OH reduction is the potential determining step. We find that the most stable species after first proton transfer is OOH with moderately potential-independent dissociation barrier of 0.37 eV. We have also shown that O_2 reduction proceeds via a so-called direct pathway, with negligible amount of peroxide produced in agreement with experimental observation [41]. We showed that there are only small reaction barriers for proton transfer and subsequent surface diffusion. This allowed us to deconvolute the overall reaction into potential dependent charge transfer to the surface and potential-independent proton transfer parallel to the surface. Since the barriers are small we can treat the potential dependent step to be the same for all four electron transfer reactions. We consider surface proton transfer to the ORR intermediates via half dissociated water network. Direct transfer of proton to one of the ORR intermediates could yield smaller barrier, however, since the barriers for the transfer via surface are already small, this will not affect the conclusions of this study.

Acknowledgements

CAMD is funded by the Lundbeck foundation. The Catalysis for Sustainable Energy initiative is funded by the Danish Ministry of Science, Technology and Innovation. This work was supported by the Danish Center for Scientific Computing. Support from the Danish Council for Technology and Innovation's FTP program and the Strategic Electrochemistry Research Center is acknowledged.

References

[1] H.A. Gasteiger, S.S. Kocha, B. Sompalli, F.T. Wagner, Appl. Catal. B: Environ. 56 (2005) 9.
[2] J. Rossmeisl, G.S. Karlberg, T. Jaramillo, J.K. Nørskov, Faraday Discuss. 140 (2008) 337.
[3] J.X. Wang, N.M. Markovic, R.R. Adzic, J. Phys. Chem. B 108 (2004) 4127.
[4] J. Rossmeisl, Á. Logadóttir, J.K. Nørskov, Chem. Phys. 319 (2005) 178.
[5] J.K. Nørskov, J. Rossmeisl, A. Logadottir, L. Lindqvist, J.R. Kitchin, T. Bligaard, H. Jónsson, J. Phys. Chem. B 108 (2004) 17886.
[6] J. Rossmeisl, Z.-W. Qu, H. Zhu, G.-J. Kroes, J.K. Nørskov, J. Electroanal. Chem. 607 (2007) 83.
[7] V.R. Stamenkovic, B.S. Moon, K.J.J. Mayrhofer, P.N. Ross, N.M. Markovic, J. Rossmeisl, J. Greeley, J.K. Nørskov, Angew. Chem. Int. Ed. 45 (2006) 2897.
[8] J. Greeley, I.E.L. Stephens, A.S. Bondarenko, T.P. Johansson, H.A. Hansen, T.F. Jaramillo, J. Rossmeisl, I. Chorkendorff, J.K. Nørskov, Nat. Chem. 1 (2009) 552.
[9] U. Nilekar, M. Mavrikakis, Surf. Sci. 602 (2008) 89.
[10] M.J. Janik, C.D. Taylor, M. Neurock, J. Electrochem. Soc. 156 (2009) 126.
[11] H.A. Hansen, J. Rossmeisl, J.K. Nørskov, Phys. Chem. Chem. Phys. 10 (2008) 3722.
[12] B. Hammer, L.B. Hansen, J.K. Nørskov, Phys. Rev. B 59 (1999) 7413.
[13] H.J. Monkhorst, J.D. Pack, Phys. Rev. B 13 (1976) 5188.
[14] D. Vanderbilt, Phys. Rev. B 41 (1990) 7892.
[15] H. Jónsson, G. Mills, K.W. Jacobsen, in: B.J. Berne, G. Ciccotti, D.F. Coker (Eds.), Classical and Quantum Dynamics in Condensed Phase Simulations, World Scientific, Singapore, 1998.
[16] G. Henkelman, H. Jónsson, J. Chem. Phys. 113 (2000) 9978.
[17] M. Dion, H. Rydberg, E. Schröder, D.C. Langreth, B.I. Lundqvist, Phys. Rev. Lett. 92 (2004) 246401.
[18] Y. Zhang, W. Yang, Phys. Rev. Lett. 80 (1998) 890.
[19] Dacapo pseudopotential code, URL: https://wiki.fysik.dtu.dk/dacapo, Center for Atomic Scale Materiale Design (CAMD), Technical University of Denmark, Lyngby.
[20] J.J. Mortensen, L.B. Hansen, K.W. Jacobsen, Phys. Rev. B 71 (2005) 035109.

[21] Atomic Simulation Environment (ASE), URL: https://wiki.fysik.dtu.dk/ase, Center for Atomic Scale Materiale Design (CAMD), Technical University of Denmark, Lyngby.
[22] H. Ogasawara, B. Brena, D. Nordlund, M. Nyberg, A. Pelmenschikov, L.G.M. Petterson, A. Nilsson, Phys. Rev. Lett. 89 (2002) 276102.
[23] T. Schiros, L.-Å. Näslund, K. Andersson, J. Gyllenpalm, G.S. Karlberg, M. Odelius, H. Ogasawara, L.G.M. Pettersson, A. Nilsson, J. Phys. Chem. C 111 (2007) 15003.
[24] A. Michaelides, P. Hu, J. Chem. Phys. 114 (2001) 1.
[25] P.J. Feibelman, Science 295 (2002) 99.
[26] A. Roudgar, A. Groß, Chem. Phys. Lett. 409 (2005) 157.
[27] S. Schnur, A. Groß, New J. Phys. 11 (2009) 125003.
[28] A. Michaelides, A. Alavi, D.A. King, Phys. Rev. B 64 (2004) 113404.
[29] J. Rossmeisl, J.K. Nørskov, C.D. Taylor, M.J. Janik, M. Neurock, J. Phys. Chem. B 110 (2006) 21833.
[30] C. Clay, S. Haq, A. Hodgson, Phys. Rev. Lett. 92 (2004) 46102.
[31] G.S. Karlberg, G. Wahnström, Phys. Rev. Lett. 92 (2004) 136103.
[32] G.S. Karlberg, G. Wahnström, J. Chem. Phys. 122 (2005) 194705.
[33] G.S. Karlberg, T.F. Jaramillo, E. Skúlason, J. Rossmeisl, T. Bligaard, J.K. Nørskov, Phys. Rev. Lett. 99 (2007) 126101.
[34] N.M. Markovic, H.A. Gasteiger, P.N. Ross, J. Phys. Chem. 99 (1995) 3411.
[35] H. Noguchi, T. Okada, K. Uosaki, Faraday Discuss. 140 (2009) 125.
[36] M. Wakisaka, H. Suzuki, S. Mitsui, H. Uchida, M. Watanabe, J. Phys. Chem. C 112 (2008) 2750.
[37] E. Skúlason, G.S. Karlberg, J. Rossmeisl, T. Bligaard, J. Greeley, H. Jónsson, J.K. Nørskov, Phys. Chem. Chem. Phys. 9 (2007) 3241.
[38] J. Rossmeisl, E. Skúlason, M.E. Björketun, V. Tripkovic, J.K. Nørskov, Chem. Phys. Lett. 466 (2008) 68.
[39] A. Michaelides, P. Hu, J. Am. Chem. Soc. 123 (2001) 4235.
[40] G.S. Karlberg, J. Rossmeisl, J.K. Nørskov, Phys. Chem. Chem. Phys. 9 (2007) 5158.
[41] B.N. Grgur, N.M. Markovic, P.N. Ross, Can. J. Chem. 75 (1997) 1465.
[42] F. Tian, R. Jinnouchi, A.B. Anderson, J. Chem. Phys. 113 (2009) 17484.
[43] F. Abild-Pedersen, J. Greeley, F. Studt, J. Rossmeisl, T.R. Munter, P.G. Moses, E. Skulason, T. Bligaard, J.K. Nørskov, Phys. Rev. Lett. 99 (2007) 016105.
[44] K.Y. Yeh, S.A. Wasileski, M.J. Janik, Phys. Chem. Chem. Phys. 11 (2009) 10108.